Electrical Power and Energy Systems 170 (2025) 110896

Contents lists available at ScienceDirect

International Journal of Electrical Power and Energy Systems

journal homepage: www.elsevier.com/locate/ijepes

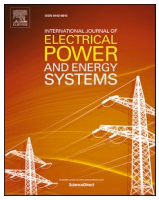

A virtual-component-embedded equivalent circuit model for lithium-ion battery state estimation

Zelin Guo [a,b], Yiyan Li [a,b,c,*], Zhenghao Zhou [a,b], Chen Zhang [a,b], Zheng Yan [b,c], Mo-Yuen Chow [d]

[a] College of Smart Energy, Shanghai Jiao Tong University, Shanghai 200240, China
[b] Shanghai Non-Carbon Energy Conversion and Utilization Institute, Shanghai Jiao Tong University, Shanghai 200240, China
[c] The Key Laboratory of Control of Power Transmission and Conversion, Ministry of Education, Shanghai Jiao Tong University, Shanghai 200240, China
[d] University of Michigan – Shanghai Jiao Tong University Joint Institute, Shanghai Jiao Tong University, Shanghai 200240, China

ARTICLE INFO

Keywords:
Battery modeling and state estimation
Equivalent circuit model
Frequency-domain multi-layer perceptron
Hybrid modeling
Iterative training strategy

ABSTRACT

Accurate modeling of batteries is the preconditon for Battery Management Systems. However, under conditions such as battery aging, low temperatures and volatile charge/discharge cycles, Equivalent Circuit Model (ECM) tends to generate significant estimation errors due to limited flexibility, while data-driven models such as neural networks lack sufficient stability and interpretability. This study proposes a novel hybrid modeling strategy for lithium-ion batteries by embedding advanced neural network modules into the classical ECM as "*virtual electronic components*", which is considered efficient, accurate and interpretable. First, the proposed hybrid modeling strategy is introduced, where a novel Frequency-Domain Multi-Layer Perceptron for Time Series (FreTS) is introduced as the neural network module to be embedded. Second, an iterative offline training strategy is designed to train the hybrid model by merging the battery state space equation into the FreTS modules' loss function. Last, the battery online state of charge (SOC) estimation is achieved based on the proposed hybrid model to demonstrate its application value. Simulation results on two real-world battery datasets show that the proposed hybrid model can achieve 18%–75% SOC estimation error reduction under varying operating conditions and on average 62% error reduction across different aging cycles, compared with the First-Order ECM.

1. Introduction

State estimation of lithium-ion batteries, such as State of Charge (SOC) and State of Health (SOH) in electric vehicles [1] and State of Energy (SOE) in energy storage systems [2], plays a vital role in the Battery Management System (BMS) to maximize the system performance and economical values [3]. In general, the battery state estimation methods can be categorized into physics-based methods and data-driven methods [4].

Physics-based methods model the internal physical process of the lithium-ion batteries, such as the equivalent circuit model (ECM) and the electrochemical model [5]. Then the model parameters can be identified from field measurement data, based on which the battery state estimation can be further achieved. ECM has been widely studied and implemented in industry due to its simplicity, stability and interpretability, and a series of ECMs have been proposed such as the First-Order RC model [6], second-order model [7], and fractional-order model [8]. [9] uses two Generalized Super-Twisting (GST) identification algorithms to identify the resistance and capacity of the First-Order RC ECM model. Then the accurate estimation of SOC and SOH is achieved based on the High-order Sliding Mode (HOSM) observer. Also based on the First-Order RC model, [10] establishes the correlation between the mass transfer resistance and the current by analyzing the electrochemical impedance spectrum of the lithium-ion battery. Then an adaptive battery state estimator is proposed to achieve joint estimation for both SOC and the State-of-Available Power (SOAP) of the battery system. [11] achieves accurate SOC estimation by introducing an improved Extended Kalman Filter (EKF) to update the parameters of the First-Order RC ECM model according to the average SOC change. In [12], a recursive least square regression algorithm with forgetting factor is proposed to identify the parameters of a Second-Order RC ECM model online. Then the joint estimation of SOH, SOC and the State of Function (SOF) is achieved by EKF. [13] uses a fractional order battery model and the fractional order Kalman filter (FOKF) to estimate the SOC, demonstrating higher

* Corresponding author.
E-mail address: yiyan.li@sjtu.edu.cn (Y. Li).

https://doi.org/10.1016/j.ijepes.2025.110896
Received 23 April 2025; Received in revised form 1 July 2025; Accepted 8 July 2025
Available online 12 July 2025

accuracy and faster convergence than the EKF. [14] proposes an SOC and SOH co-estimation scheme using fractional-order calculus, with a fractional-order equivalent circuit model parameterized by a hybrid Genetic Algorithm (GA) and Particle Swarm Optimization (PSO) method. The dual FOKF is then applied for simultaneous SOC and SOH estimation, demonstrating high accuracy and resilience to battery aging. The performance of the physics-based methods depends heavily on the accuracy of the physical model. However, due to the complexity and nonlinearity of the battery electrochemical process, existing physical models have inevitable modeling errors. Such modeling errors will consequently lead to state estimation errors, especially under extreme operating conditions such as heavy current charging/discharging and freezing temperature environment.

Data-driven methods try to directly build the mapping from field measurement data, e.g., current, voltage and temperature, to the battery state variables by statistic models [15] or neural networks [16,17]. In [18], real-time measurements of battery voltage, current and ambient temperature are fed into a dynamically-driven recurrent network (DDRN) to estimate the SOC and SOH of the electric vehicle battery. [16] presents a novel approach for SOC estimation using Deep Feedforward Neural Networks (DNN), which directly map battery measurements to SOC. The DNN is trained with data generated under various drive cycle loads and ambient temperatures, demonstrating the ability to accurately estimate SOC across a wide range of temperatures. [19] proposes a stacked long short-term memory (sLSTM) network for accurate SOC estimation of lithium iron phosphate batteries using current, voltage, and temperature measurements, achieving root Mean Square Error (RMSE) within 2 % and Mean Average Error (MAE) within 1 %. Data-driven methods are easy to implement and can achieve higher accuracy than physics-based methods due to the strong nonlinear learning ability of the neural nets. However, data-driven methods rely heavily on the quality and quantity of the field measurement data, which impairs the model stability, interpretability and robustness.

Given that both physics-based and data-driven models have their own limitations, recent studies have increasingly focused on hybrid modeling methods, which can be categorized into three classes according to how the physical and data-driven parts are merged. *First*, neural network models are established independently and work parallelly with the physics-based models, after which a weigting mechanism is used to merge the two estimation results. For example, in [20] a fusion model integrating Convolutional Neural Networks (CNN) with a First-Order RC ECM is proposed. An adaptive weight correction method is employed to assign appropriate weights to both components to obtain the final terminal voltage prediction results. *Second*, neural networks and physical models are integrated to formulate a larger and comprehensive modeling framework. For example, in [21] two Feedforward Neural Networks (FNNs) are introduced to correct the modeling errors of the Thermal Equivalent Circuit Model with Diffusion (TECMD), formulating a hybrid modeling framework. *Third*, neural networks are used to replace the elements in the physical models to enhance the nonlinear fitting capability. Such as in [22] and [23], neural network modules are introduced to replace the resistances and capacitances in the Third-Order and First-Order RC ECM modules, respectively.

However, existing hybrid modeling strategies can hardly balance the triangle among efficiency, interpretability and accuracy, which is considered a research gap that needs to be further addressed. As mentioned above, the first hybrid modeling strategy is straightforward and easy to implement. But the neural network model is still a black box and hard to interpret. Meanwhile, the performance of the hybrid model highly relies on the weighting mechanism, which introduces additional uncertainty and instability. The second strategy is a organic combination between the physical and data-driven model, which is considered interpretable. But the resulting framework is usually overcomplex and lead to concerns on computation efficiency, considering the framework needs to be executed in real time in practice. The third strategy is indeed an ECM-structured neural network, which may have good accuracy due to the nonlinear learning ability and also has certain interpretability. However, such NN-dominated framework is demanding on data quality and may lead to unstable performances especially under abnormal working conditions.

This paper proposes a novel hybrid modeling strategy to merge the ECM and neural networks, which is considered efficient, interpretable and accurate. More specifically, advanced neural network modules, i.e. Frequency-Domain Multi-Layer Perceptron for Time Series (FreTS), are introduced and embedded into the traditional ECM. Each FreTS module is accompanied with an electronic component in ECM such as the Ohm Resistance, Polarization Resistance and Polarization Capacitance, serving as "*virtual electronic components*" to dynamically compensate the parameter estimation errors. As such, the outputs of the FreTS modules correspond to the fitting residues of the ECM components, which are considered interpretable. In this framework, the basic ECM can guarantee the model stability and accuracy even under limited data conditions. The embedded FreTS modules enhance nonlinear fitting capability and improve model performance, while maintaining interpretability at the structural level. In addition, FreTS is a lightweight neural network structure with negligible computation costs, ensuring the efficiency of the whole hybrid modeling framework when implemented in real time.

The main contributions of this paper are threefold:

- This study proposes a novel hybrid modeling framework for lithium-ion batteries by embedding neural network modules as "virtual electronic components" into the classical ECM. The neural network modules are trained to compenstate the fitting residuals of the traditional ECM, effectively enhancing the model's accuracy and flexibility under complex operating conditions while preserving the interpretability and stability of the ECM-based framework.
- This study employs the FreTS as the embedded neural network module. Compared with traditional time-domain neural networks, FreTS transforms time series data into the frequency domain, enabling more effective learning of the spatio-temporal characteristics of the series. Meanwhile, FreTS is a lightweight model with superior computation efficiency, enabling real-time battery state estimation on distributed platforms in practical applications.
- An iterative offline training strategy is developed to resolve the indirect training problem inherent in embedded FreTS modules. The battery state space equation is merged into the traditional Mean Squared Error (MSE) to estimate the terminal voltage prediction accuracy. This physics-informed loss function guides the training of the FreTS modules, ensuring that the training process is both physically constrained and interpretable.

The remainder of this paper is organized as follows. In Section 2, the classical ECM used in this paper and the parameter identification method are introduced. In Section 3, the proposed hybrid model and the parameter correction method are proposed. In Section 4, two real-world battery datasets are used to verify the accuracy of the hybrid model. Section 5 concludes this paper.

2. Basic ECM and initial parameter identification

Fig. 1 shows the overall framework of the paper. Sections 2, 3.1, and 3.2 belong to the offline training part of the proposed strategy, mainly introducing the embedding method and offline training strategy of FreTS. Section 3.3 includes the online application process of the strategy.

2.1. Basic equivalent circuit model of the lithium-ion battery

Fig. 2 shows the First-Order RC ECM of the lithium-ion battery under discharging condition. The model describes the dynamic polarization characteristics of the battery by a RC circuit, and the basic circuit elements include R_0, R_D, C_D. R_0 is the ohmic internal resistance, R_D is the

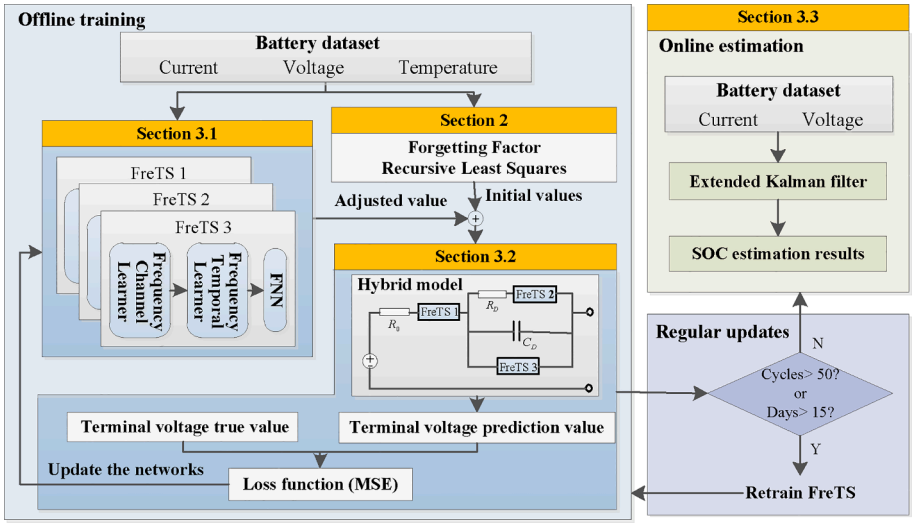

Fig. 1. Overall framework of the paper.

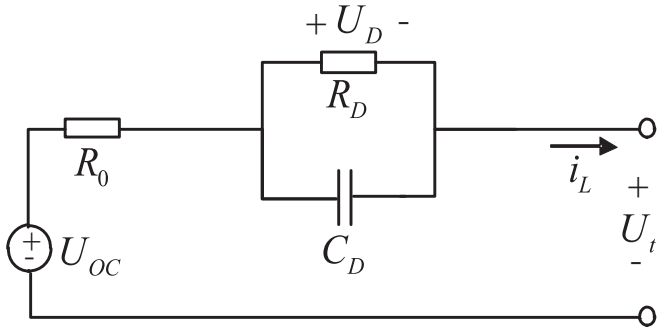

Fig. 2. First-Order RC ECM of the battery.

polarization resistance, and C_D is the battery capacitance. The simplest first-order RC ECM serves as the foundation for illustrating the hybrid model's formulation and training methodology. Note that such a hybrid modeling strategy can be easily extended to more complicated ECMs such as the Second-Order RC ECM or the Fractional-Order ECM.

When the battery is discharged, the state space equation of the First-Order RC ECM can be described as

$$\begin{cases} \dfrac{dU_D}{dt} = \dfrac{i_L}{C_D} - \dfrac{U_D}{R_D C_D} \\ U_t = U_{OC} - U_D - i_L R_0 \end{cases} \tag{1}$$

where U_D is the voltage of the $R_D C_D$ parallel part, i_L is the battery discharging current, U_t is the terminal voltage of the battery, U_{OC} is the open circuit voltage of the battery and is a function of the battery SOC

$$U_{OC} = f(SOC) \tag{2}$$

where $f(\cdot)$ is a polynomial function affected by temperature, which can be established by pre-experiments. Because SOC is not measurable, the SOC is calculated by the ampere-hour integration

$$SOC(t) = SOC(0) - \int_0^t \frac{i_L dt}{C_b} \tag{3}$$

where $SOC(0)$ is the initial SOC value when the battery starts discharging. C_b is the maximum available capacity of the battery under the current discharging cycle.

2.2. Initial parameter identification

In this paper, the parameter identification results of the traditional ECM are called the *initial parameters* (i.e. the parameters that have not been corrected by the FreTS modules). The initial parameters can be obtained online based on field measurements by using the recursive least squares method with forgetting factor (FFRLS). Details of FFRLS can be found in [24]. The First-Order RC ECM equation in (1) can be transformed into the least-squares form as

$$y_k = \theta_k \phi_k \tag{4}$$

$$\theta_k = \begin{bmatrix} \dfrac{T - 2R_D C_D}{T + 2R_D C_D} \\ \dfrac{R_0 T + R_D T + 2R_0 R_D C_D}{T + 2R_D C_D} \\ \dfrac{R_0 T + R_D T - 2R_0 R_D C_D}{T + 2R_D C_D} \end{bmatrix}^T \tag{5}$$

$$\phi_k = [\, -y_{k-1} \quad I_k \quad I_{k-1} \,]^T$$

where y_k is the output of the system, i.e. $U_t - U_{OC}$ in this paper. θ_k is the parameter matrix and ϕ_k is the data matrix. T is the sampling interval ($T = 1$ s in this paper). I_k is the discretized expression of the current i_L.

The parameter optimization process of FFRLS is as follows

$$\begin{cases} \widehat{\theta}_k = \widehat{\theta}_{k-1} + K_k(y_k - \phi_k \widehat{\theta}_{k-1}) \\ K_k = \dfrac{P_{k-1}\theta_k}{\lambda + \phi_k P_{k-1} \phi_k^T} \\ P_k = \dfrac{(I - K_k \phi_k) P_{k-1}}{\lambda} \end{cases} \tag{6}$$

where λ is the forgetting factor, $\widehat{\theta}$ is the estimated value of the parameter matrix, K_k is the gain matrix, P_k is the covariance matrix, I is the identity matrix.

FFRLS updates the model parameters at each time step to obtain the initial parameter identification results.

3. Hybrid model and parameter correction

3.1. FreTS-Embedded equivalent circuit model

When the battery works in complex conditions such as freezing

temperature or heavy charging/discharging mode, the electrochemical process of the battery becomes rather complex and nonlinear, leading to risks of large fitting errors of the ECMs. In this section, the proposed approach merges three FreTS modules (i.e. FreTS1, FreTS2, FreTS3) into the First-Order RC ECM to enhance its adaptability and flexibility, as shown in Fig. 3.

FreTS is designed as time series regression architecture based on frequency-domain MLP, leveraging the frequency-domain information of time series to address regression tasks [25]. Compared to traditional MLPs, FreTS effectively captures the intrinsic periodicity and frequency-domain features of the data. Its frequency-sensing module significantly reduces redundant computations, enhancing efficiency. With superior generalization and lightweight design, FreTS is well-suited for deployment in practical battery applications.

For a time series $[H_1, H_2, \cdots, H_T] \in \mathbb{R}^{N\times T}$, consisting of N series and T timestamps, FreTS transforms the data from the time domain to the frequency domain using the Discrete Fourier Transform (DFT)

$$H_{chan} = DFT(H) = \mathrm{Re}(H_{chan}) + j\mathrm{Im}(H_{chan}) \tag{7}$$

The frequency channel learner in FreTS models the dependencies between sequences

$$\begin{aligned} Z_{chan} = {} & \sigma_{chan}(\mathrm{Re}(H_{chan})W_\tau - \mathrm{Im}(H_{chan})W_i + B_\tau) + j\sigma(\mathrm{Re}(H_{chan})W_i \\ & + \mathrm{Im}(H_{chan})W_\tau + B_i) \end{aligned} \tag{8}$$

where W_τ, W_i are the real and imaginary parts of the weight matrix in the frequency channel learner. B_τ, B_i are the corresponding real and imaginary parts of the bias. σ_{chan} is the activation function. Then the frequency domain output Z_{chan} is transformed back to the time domain using the inverse Discrete Fourier Transform (IDFT)

$$Z = IDFT(Z_{chan}) \tag{9}$$

The frequency temporal learner in FreTS models the time dependence of a single time series

$$Z_{temp} = DFT(Z) = \mathrm{Re}(Z_{temp}) + j\mathrm{Im}(Z_{temp}) \tag{10}$$

$$\begin{aligned} S_{temp} = {} & \sigma_{temp}(\mathrm{Re}(Z_{temp})W_k - \mathrm{Im}(Z_{temp})W_j + B_k) + j\sigma(\mathrm{Re}(Z_{temp})W_j \\ & + \mathrm{Im}(Z_{temp})W_k + B_j) \end{aligned} \tag{11}$$

where W_j, W_k are the real and imaginary parts of the weight matrix in the frequency temporal learner. B_j, B_k are the corresponding real and imaginary parts of the bias. σ_{temp} is the activation function. Then the frequency domain output S_{temp} is transformed back to the time domain using the inverse Discrete Fourier Transform (IDFT)

$$S = IDFT(S_{temp}) \tag{12}$$

Finally, FreTS uses a simple FNN to map the learned features to the network output

$$Y = \sigma_{FNN}(S\phi_1 + b_1)\phi_2 + b_2 \tag{13}$$

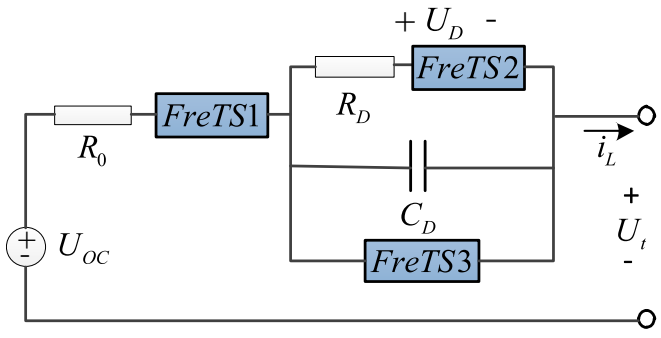

Fig. 3. Structure of the hybrid model.

where ϕ_1, ϕ_2, b_1, b_2 are the weight matrix and bias of the FNN, σ_{FNN} is the activation function of the FNN, Y is the output of the FNN.

The inputs are field measurements $i_{L,t}$, U_t and $Temp_t$, while the outputs, denoted by R_{0_F}, R_{D_F}, C_{D_F}, are expected to be the corrections for the initial parameters. It is expected that the FreTS modules can correct the initial parameter estimation errors to improve the modeling accuracy. Then the final parameter identification results of the hybrid model can be expressed by

$$\begin{cases} \widetilde{R}_0 = R_{0\_FFRLS} + R_{0\_F} \\ \widetilde{R}_D = R_{D\_FFRLS} + R_{D\_F} \\ \widetilde{C}_D = C_{D\_FFRLS} + C_{D\_F} \end{cases} \tag{14}$$

where $\widetilde{R}_0$, $\widetilde{R}_D$, $\widetilde{C}_D$ are the parameter values after correction. Accordingly, the state space equation of the hybrid model can be rewritten as

$$\begin{cases} \dfrac{dU_D}{dt} = \dfrac{i_L}{\widetilde{C}_D} - \dfrac{U_D}{\widetilde{R}_D\widetilde{C}_D} \\ U_t = U_{OC} - U_D - i_L\widetilde{R}_0 \end{cases} \tag{15}$$

The architecture of the FreTS modules is shown in Fig. 4.

3.2. Offline training strategy of the hybrid model

The FreTS modules cannot be trained directly as a typical regression problem because the outputs, i.e. R_{0_F}, R_{D_F}, C_{D_F} , are not measurable. However, the predicted value of the battery terminal voltage U_t^{pre} can be calculated based on Eq. (15), and then indirectly estimate the FreTS modules performance by comparing U_t^{pre} with the ground truth U_t. Following this idea, this study merges the state space equation of the First-Order RC ECM into the loss function to train the FreTS modules.

Specifically, the outputs of the three FreTS modules are used as the adjusted values of the parameters, and the corrected values of the parameters are calculated according to (14). The corrected values of the parameters are then fed into the battery state space equation to calculate the predicted value of the battery terminal voltage. Finally, the mean square error (MSE) between the predicted values of the hybrid model's terminal voltage and the actual values of the battery's terminal voltage was calculated, and it was used as a new loss function to participate in the backpropagation process of the three FreTS modules.

To facilitate the program calculation, the state space equation of (15) needs to be discretized as

$$\begin{aligned} U_D(k+1) &= e^{-\frac{1}{\widetilde{R}_D(k)\widetilde{C}_D(k)}}\cdot U_D(k) + \widetilde{R}_D(k)\left(1 - e^{-\frac{1}{\widetilde{R}_D(k)\widetilde{C}_D(k)}}\right)\cdot i_L(k) \\ U_t^{pre}(k+1) &= U_{OC}(k+1) - i_L(k+1)\cdot\widetilde{R}_0(k+1) - U_D(k+1) \end{aligned} \tag{16}$$

The modified loss function is described as

$$loss = \frac{1}{n}\sum_{i=1}^{n}\left(U_{t,i}^{pre} - U_{t,i}^{true}\right)^2 \tag{17}$$

where $U_{t,i}^{pre}$ is the predicted value of the terminal voltage of the hybrid model at time i, $U_{t,i}^{true}$ is the actual value of the terminal voltage of the battery at time i, n is the number of sample points.

To summarize, the offline training strategy of the hybrid model is shown in Fig. 5, including the following steps:

1) Forward calculation. After initialization of the FreTS modules, the input variables (i.e., current, voltage, and temperature) are fed into the modules to obtain their outputs.

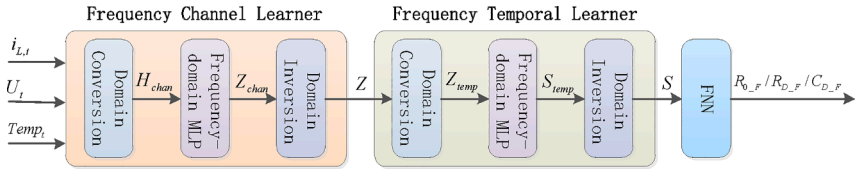

Fig. 4. The FreTS architecture.

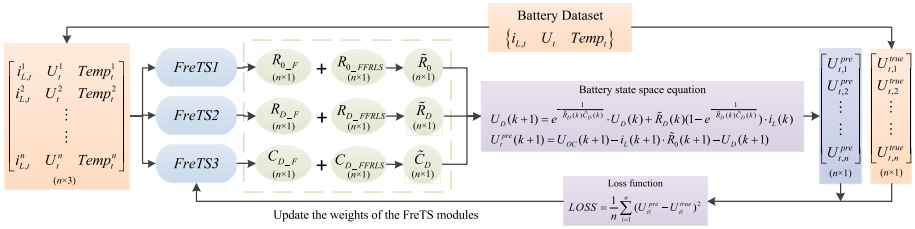

Fig. 5. Training strategy of the hybrid model.

2) Parameter correction. The outputs of FreTS modules are used to correct the initial parameter estimation results, shown as equation (14).
3) Loss calculation. The corrected parameters in step 2) are then fed into the discretized state space equation in (16) to obtain the predicted value of the terminal voltage $U_{t,i}^{pre}$. The MSE loss can be calculated by comparing $U_{t,i}^{pre}$ with the ground truth $U_{t,i}^{true}$.
4) Back propagation. Based on the loss in step 3), the parameters of the FreTS modules can be updated via the back-propagation process.
5) Stopping criteria. Step 1)–4) continues iteratively until $U_{t,i}^{pre}$ is close enough to $U_{t,i}^{true}$ with a certain quantitative criteria. Then the FreTS modules are considered well-trained to fit the ECM residuals, and the training process will end. The parameters obtained from offline training will be applied to online SOC estimation.

Note that the parameters obtained by offline training will not be updated in the online battery SOC estimation stage, due to considerations of the model training cost. Instead, the model undergoes periodic retraining using the latest field measurement data to maintain accuracy. For example, considering the battery parameters will drift along with the charging/discharging cycles [26] and the self-discharging behaviors [27], the FreTS modules are retrained every 50 cycles or 15 days for parameter updates.

3.3. Online SOC estimation for lithium batteries

EKF is a nonlinear extension of the standard Kalman filter [28], and the calculation process is divided into prediction phase and update phase.

In the prediction phase, based on the estimated value $\hat{x}_{k-1}$ of the system state at time k-1, the prior estimate $\hat{x}_{k|k-1}$ of the system state at time k and the covariance matrix $P_{k|k-1}$ of the prediction error of the state variable is calculated

$$\hat{x}_{k|k-1} = g(\hat{x}_{k-1}, u_{k-1}) \tag{18}$$

$$P_{k|k-1} = cov(x_k - \hat{x}_{k|k-1}) = A_{k-1}P_{k-1}A_{k-1}^T + Q_{k-1} \tag{19}$$

where $g(\cdot)$ is the state transition function of the system, u_{k-1} is the input to the system, x_k is the estimate of the state of the system at time k, A_{k-1} is the state transition matrix, P_{k-1} is the error covariance matrix at time k-1, Q_{k-1} is the covariance matrix of the process noise.

In the correction phase, the Kalman gain matrix K_k is calculated and the state variables and covariance matrix are corrected as

$$K_k = P_{k|k-1}C_k^T\left(C_kP_{k|k-1}C_k^T + R\right)^{-1} \tag{20}$$

$$\hat{x}_k = \hat{x}_{k|k-1} + K_k\left[y_k - h\left(\hat{x}_{k|k-1}, u_k\right)\right] \tag{21}$$

$$P_k = (I - K_kC_k)P_{k|k-1} \tag{22}$$

where C_k is the output matrix, R is the covariance matrix of the observation noise, y_k is the actual output of the system, $h(\cdot)$ is the output equation of the system, I is the identity matrix.

When P_k is minimized, the optimal estimate of the state variable is obtained.

In online application stage, based on the battery equation established by offline training and the real-time measurements of the battery voltage, the online estimation of SOC can be obtained by EKF.

In this paper, RMSE [29] and Mean Absolute Percentage Error (MAPE) are used to calculate the error, which can be described as

$$RMSE = \sqrt{\frac{1}{m}\sum_{i=1}^{m}\left(\tilde{z}_i - z_i\right)^2} \tag{23}$$

$$MAPE = \frac{1}{m}\sum_{i=1}^{m}\left|\frac{\tilde{z}_i - z_i}{z_i}\right| \times 100 \tag{24}$$

where m is the number of sample points, $\tilde{z}_i$ is the predicted value, z_i is the actual value.

4. Results and analysis

4.1. Comparison of modeling methods under varying temperature and operating conditions

4.1.1. Test case setup

To verify the accuracy of the proposed hybrid model, the test case is established using a real-world battery dataset provided by [30]. This dataset includes charging/discharging measurements, e.g. current, voltage, cell temperature, from a Panasonic 18650PF cell under different working conditions. Details of the battery is shown in Table 1.

This section examines five distinct operating conditions: HWFET [31], US06 [32], CYCLE1, CYCLE2, and CYCLE3, at 4 different ambient temperatures: −10 °C, 0 °C, 10 °C, and 25 °C (i.e. 5 × 4 = 20 scenarios), to comprehensively evaluate the model performance. Among these, HWFET and US06 are smooth and sharp standard driving cycles, respectively, while CYCLE1–3 are random mixes of US06, HWFET,

Table 1
Panasonic 18650PF cell information.

Parameter	Value
Type	18650PF
Rated capacity	2.9 Ah
Minimum capacity	2.75 Ah
Terminal voltage range	2.5 V–4.2 V
Temperature of discharge	−20 °C to 60 °C

Table 2
Hyperparameters for the FreTS module.

Hyperparameters	FreTS1	FreTS2	FreTS3
Number of embed-layer nodes	16	16	64
Number of hidden-layer nodes	32	64	128
Number of training epochs	200	200	200
Initial learning rate	0.0001	0.0001	0.0001
Optimizer	Adagrad	Adagrad	Adam

UDDS [33], and LA92 [34].

As an example, Fig. 6 shows the pulse current curve of the battery when discharging at 10 °C, and the voltage and SOC profiles when discharging at four temperatures, all under the HPPC operating condition.

As shown in Fig. 6, the ambient temperature shows significant impact on the discharging performance of the battery: the lower the temperature, the faster the battery SOC curve decreases, resulting in worse discharging performance. Accordingly, the battery parameters are also dependent on the ambient temperature, making the battery parameter identification results at 10 °C not applicable to the same battery at −10 °C.

The configuration of the three FreTS modules are shown in Table 2. Hyperparameters are determined based on trial-and-error strategy to maximize the model performance.

It should be mentioned that in order to speed up the model training, the original measurements are re-sampled at lower frequency (6 s in this section) to obtain the current, voltage and cell temperature data. The SOC values of the battery can be calculated according to (3).

4.1.2. Accuracy verification of the hybrid model

This section first compares the parameter identification results between the classical First-Order RC ECM and the proposed hybrid model. The parameters to be identified include the ohmic internal resistance R_0, the polarization resistance R_D and the polarization capacitance C_D. The dataset used is the field measurement data introduced in Section 4.1.1. Fig. 7 shows the identification results of battery parameters at different temperatures under HWFET operating condition.

To further validate the model accuracy, the predicted terminal voltage $U_{t,i}^{pre}$ is calculated based on the First-Order RC ECM, FreTS, and the proposed hybrid model with the identified parameters, respectively. The hyperparameters for FreTS are consistent with those of FreTS3 in Table 2, where the inputs are current, temperature, and discharge capacity, and the output is voltage.

The research compares the performance of First-Order RC ECM, FreTS, and the proposed hybrid model in fitting the actual value of battery terminal voltage under 20 scenarios, respectively. Simulation results are summarized in Fig. 8, for better visualization, the fit results of the First-Order RC ECM and hybrid model are plotted by sampling the data every 60 s.

In Table 3, this study calculates the RMSE of the First-Order RC ECM, FreTS, and the hybrid model to make a quantitative performance comparison. Fig. 9 shows the RMSE improvement of the hybrid model compared to the First-Order RC ECM.

The results support these observations:

- As shown in Fig. 8, the comparison results of terminal voltages in 20 scenarios show that the hybrid model has better fitting ability than the First-Order RC ECM. Especially in the middle stage of battery discharge, the hybrid model is better able to follow the rapid fluctuation of the actual value of battery voltage. Rapid (e.g., US06) and irregular(e.g., CYCLE1-3) discharge conditions limit the ability of First-Order RC ECM to accurately capture the real behavior of the battery. Introducing FreTS modules can significantly mitigate this issue by mapping real-time dynamic characteristics, such as battery current and temperature, to the battery parameters (as shown in Fig. 7). This approach enhances the flexibility and accuracy of the hybrid model under complex and fluctuating conditions.
- The fitting accuracy of the First-Order RC ECM decreases with lower temperatures, leading to larger fitting errors. As shown in Fig. 9, the hybrid model enhances the performance of the First-Order RC ECM under various temperature conditions, with the improvement being more pronounced at lower temperatures.
- Under the same network structure, the hybrid model outperforms FreTS, suggesting that its fitting performance is not solely derived from FreTS, but results from the combined strengths of both the First-Order RC ECM and FreTS. The First-Order RC ECM-based circuit structure provides the hybrid model with fundamental stability and accuracy, as well as enhanced interpretability, in contrast to the 'black-box' nature of FreTS. Moreover, the incorporation of FreTS modules offers a positive corrective effect on the accuracy of the First-Order RC ECM.

To evaluate the sensitivity of the hybrid model to initial parameters, the US06 operating condition at −10 °C is selected. By maintaining all other conditions constant, three different forgetting factors (0.95, 1, and 1.05) are applied in the FFRLS method to generate three distinct sets of initial parameter combinations.

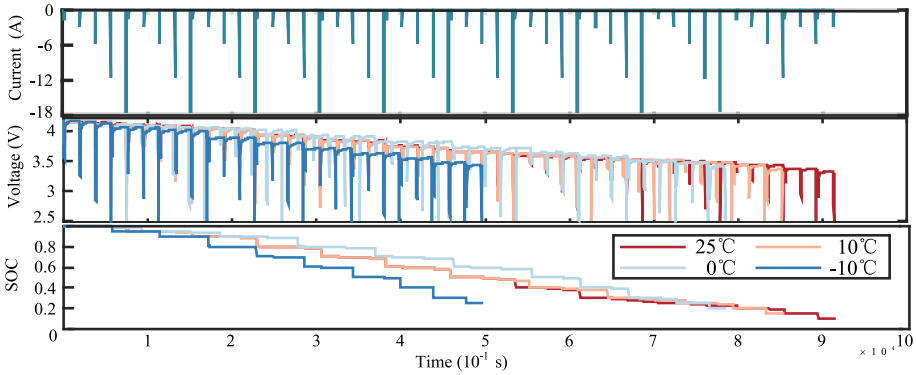

Fig. 6. The pulse current curve of the battery when discharging at 10 °C, and the changes of the voltage and SOC when discharging at four temperatures.

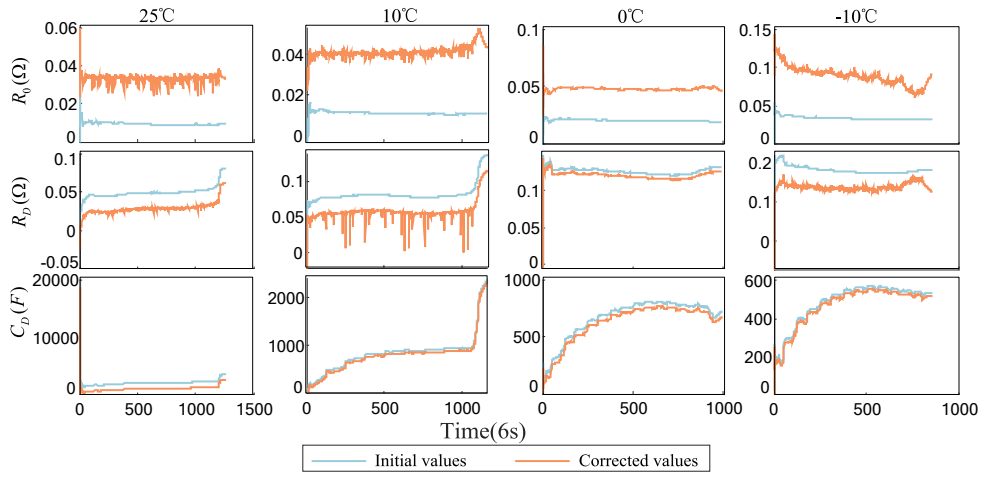

Fig. 7. Identification results of battery parameters at different temperatures under HWFET operating mode.

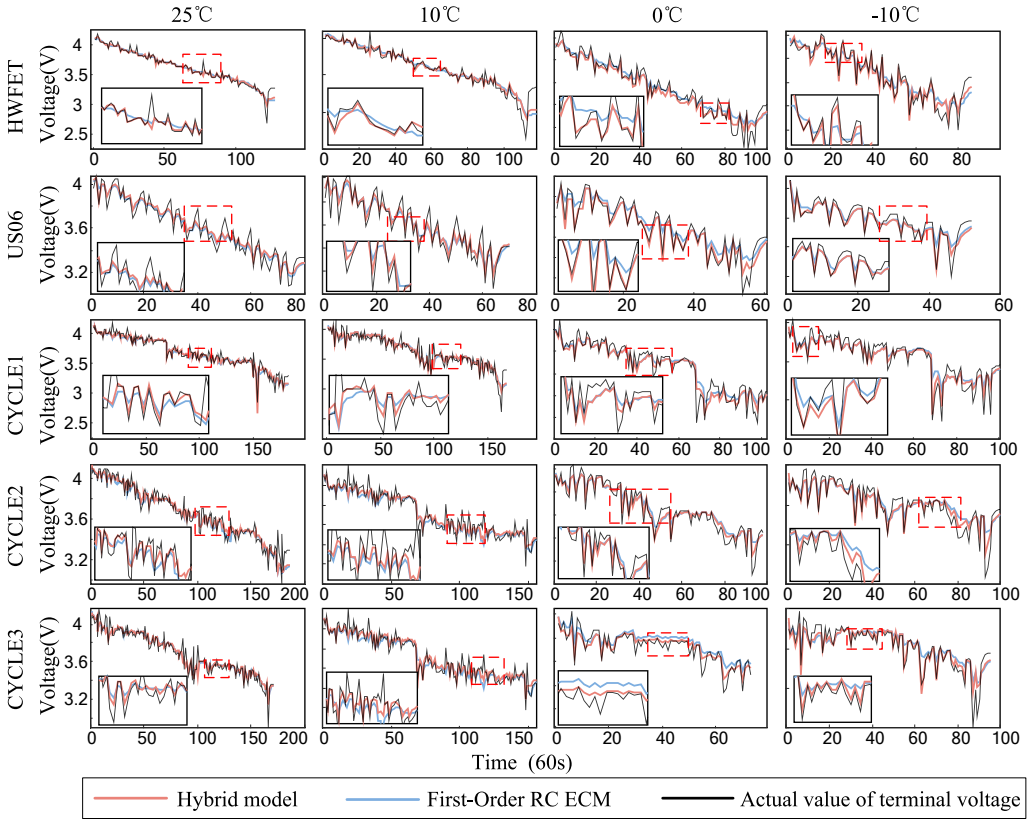

Fig. 8. Comparison between the terminal voltage predictions and the ground truth, under different operating conditions and ambient temperatures.

Fig. 10 shows the error distribution of voltage and the percentage improvement in RMSE for these three sets of initial parameter combinations. The improvement percentages are 33.7 %, 39.4 %, and 33.9 %, respectively. The results indicate that the accuracy of the hybrid model is influenced by different combinations of initial parameters, and the model's accuracy decreases when the initial parameter combination has a larger error. Despite significant errors in the initial parameter combinations, the hybrid model still achieves an RMSE improvement of 30 % to 40 %.

4.1.3. SOC estimation results

Based on the parameter identification results in Section 4.1.2, this study further implement EKF to estimate the battery SOC during the discharging process to demonstrate the application value of the proposed hybrid model. Fig. 11 shows the SOC estimation results under 20 scenarios, based on the First-Order RC ECM and the proposed hybrid model with their identified parameters, respectively. The results support these observations:

Table 3
RMSE calculation results.

Temp	Comparison models	Operating condition				
		HWFET	US06	CYCLE1	CYCLE2	CYCLE3
25 °C	First-Order RC ECM	0.0648	0.0976	0.0723	0.0787	0.0618
	FreTS	0.0733	0.1068	0.0664	0.0919	0.0634
	Hybrid model	0.0555	0.0876	0.0587	0.0702	0.0580
10 °C	First-Order RC ECM	0.0941	0.1172	0.0952	0.0801	0.0792
	FreTS	0.1042	0.1038	0.0911	0.1068	0.0636
	Hybrid model	0.0800	0.0992	0.0825	0.0708	0.0567
0 °C	First-Order RC ECM	0.0724	0.1312	0.0780	0.0717	0.0815
	FreTS	0.0900	0.1078	0.0862	0.0697	0.0901
	Hybrid model	0.0544	0.0785	0.0620	0.0468	0.0543
−10 °C	First-Order RC ECM	0.0835	0.1525	0.1095	0.1228	0.1292
	FreTS	0.0817	0.1356	0.1067	0.0964	0.1192
	Hybrid model	0.0495	0.1022	0.0746	0.0804	0.0766

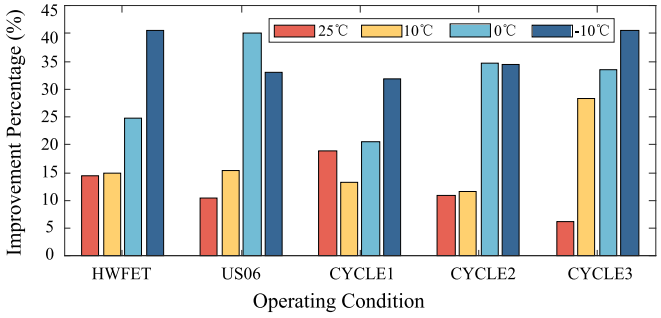

Fig. 9. RMSE improvement of the hybrid model compared to the First-Order RC ECM.

- Overall speaking, the proposed hybrid model shows better SOC estimation accuracy than the First-Order RC ECM at all scenarios, especially at lower temperatures and rapid and complex conditions. Such an observation is consistent with the model accuracy comparison results in Section 4.1.2.
- The First-Order RC ECM suffers from error increase as the discharging process evolves, especially under US06, CYCLE1, and CYCLE3 operating condition. This again shows the advantages of the parameter error compensation and nonlinear fitting capabilities of the proposed hybrid model.

Note that the proposed hybrid model does not always outperform the First-Order RC ECM. For example, the hybrid model shows larger SOC estimation errors at early stages under CYCLE3 mode (0 °C, −10 °C). During FreTS module training, the loss function is to minimize the global estimation errors during the whole discharging period, during which process some local estimation accuracies are sacrificed. Nonetheless, as shown in Table 4, the hybrid model produces a lower proportion of samples with errors exceeding 0.05 compared to the First-Order RC ECM, which meets the accuracy requirements for practical BMS applications.

Fig. 12 shows the boxplot of the error distribution for the SOC estimation results of the hybrid model and the First-Order RC ECM. The hybrid model exhibits consistently lower and more concentrated median SOC estimation errors than the ECM model, as indicated by the smaller and lower-positioned boxplots across all 20 scenarios. Furthermore, the maximum errors (upper whiskers and outliers) observed in the hybrid model are also significantly reduced, with most values remaining below 0.3, whereas ECM errors frequently exceed 0.4.

Table 5 provides a quantitative comparison for the SOC estimation accuracy by calculating RMSE and MAPE.

Table 6 shows the average time costs (25 °C, 10 °C, 0 °C, −10 °C) of offline training and online SOC estimation under US06, HWFET, and CYCLE1-3 operating conditions. The model is trained on a system equipped with a 13th Gen Intel Core i7-13700 processor (2.10 GHz) and 32.0 GB of RAM. The hybrid model requires more time during the offline training phase due to neural network training. However, since offline training only occurs after a certain number of cycles or over extended periods, its impact on practical applications is minimal. In contrast, the online training phase of the hybrid model incurs lower time costs, enabling rapid SOC estimation within seconds and thus satisfying the demands of real-world engineering applications..

4.1.4. *Cross-cycle generalization of the hybrid model*

To assess the hybrid model's capability to quickly adapt to various battery states without retraining, a cross-cycle generalization test is designed. In this test, the model is trained solely on CYCLE1 and then evaluated on CYCLE2 and CYCLE3 under identical temperature conditions, without any additional fine-tuning. Notably, CYCLE1, CYCLE2, and CYCLE3 exhibit substantial differences in discharge rate, duration,

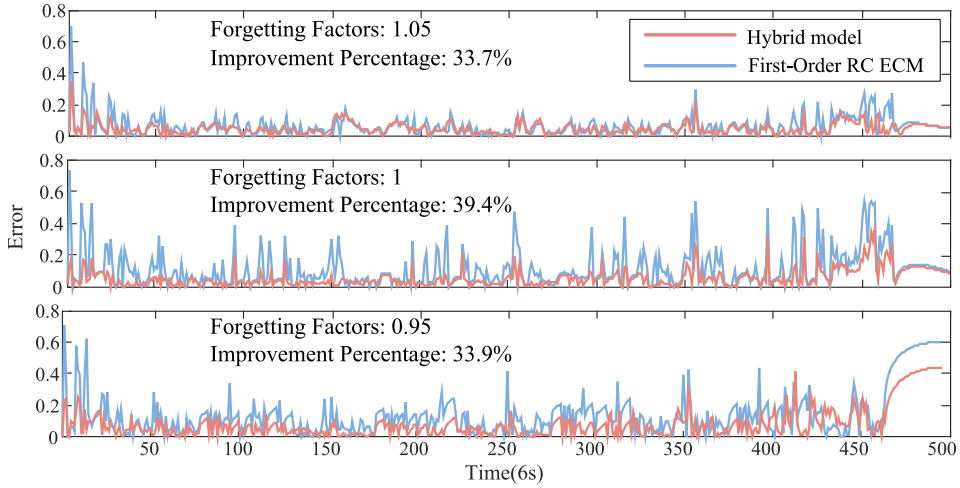

Fig. 10. Error distribution of voltage and RMSE improvement for three initial parameter combinations.

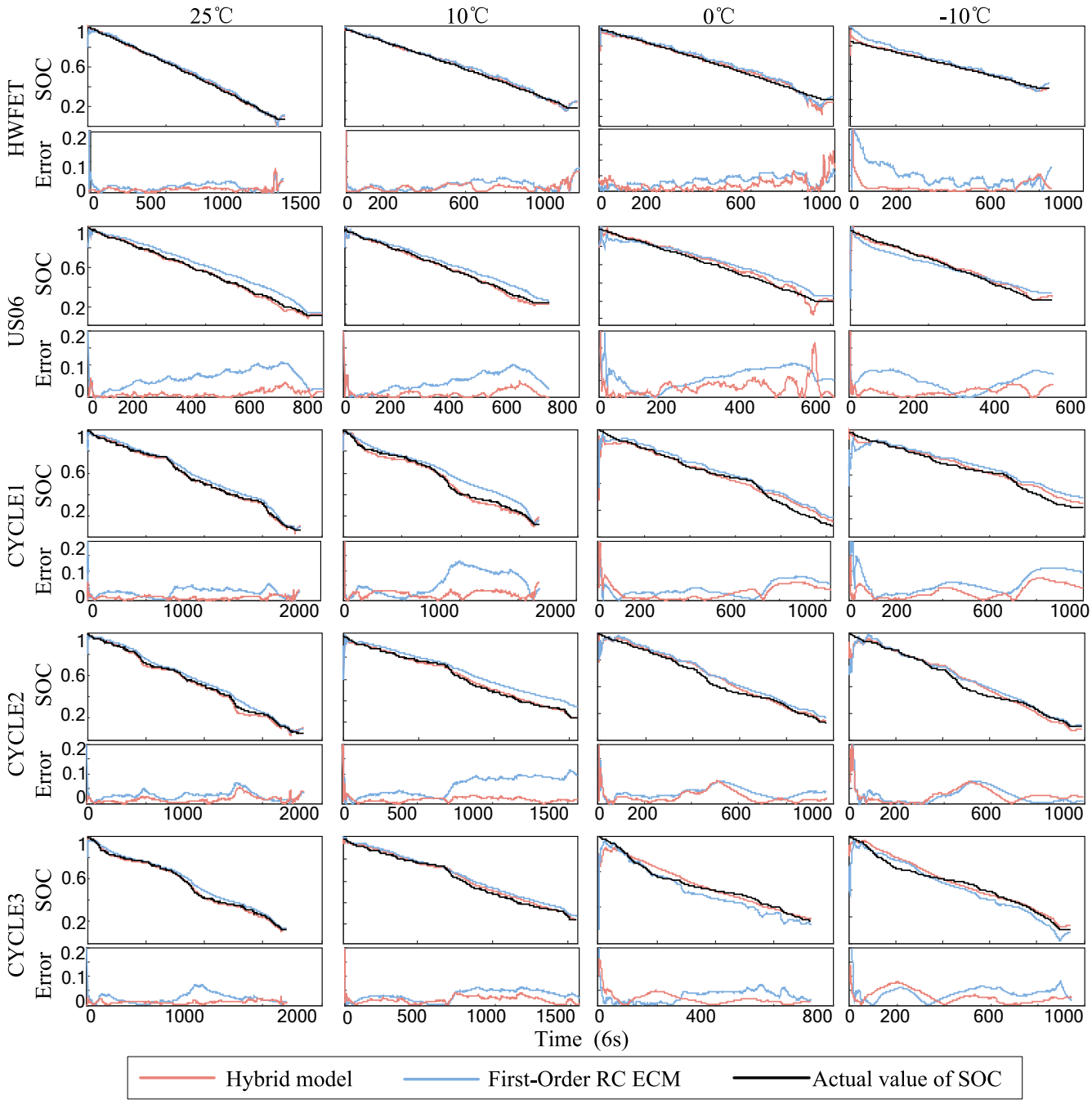

Fig. 11. SOC estimation results and the estimation errors based on First-Order RC ECM and proposed hybrid model under 20 scenarios.

and dynamic characteristics, as they are random mixtures of different standard driving conditions. This setup ensures the model has no prior exposure to CYCLE2 and CYCLE3, enabling a valid test of its cross-cycle generalization.

Table 7A shows the RMSE results of the hybrid model on CYCLE2 and CYCLE3 across four temperature settings. The consistently low error values demonstrate that the proposed model maintains high accuracy even when applied to unseen cycle data.

To further assess the impact on practical state estimation, Fig. 13 and Table 7B show the SOC estimation performance on the same test data. Both RMSE and MAPE metrics are reported. The hybrid model achieves low SOC estimation errors across all temperatures, with RMSE mostly within 1 %–3% and MAPE below 5 %. These results confirm the model's robustness and adaptability to previously unseen battery states without the need for retraining.

4.2. Comparison of modeling methods for different SOH conditions

To verify the accuracy of the hybrid model in the context of battery cycle aging, the test case is established using a real-world battery dataset

Table 4
Comparison of high-error proportions (>0.05) between hybrid model and ECM.

Temp	Comparison models	Operating condition				
		HWFET	US06	CYCLE1	CYCLE2	CYCLE3
25 °C	First-Order RC ECM	1.50 %	62.53 %	2.08 %	6.86 %	9.68 %
	Hybrid model	0.95 %	0.37 %	0.05 %	2.15 %	0.00 %
10 °C	First-Order RC ECM	3.16 %	45.19 %	46.63 %	54.74 %	28.72 %
	Hybrid model	3.15 %	1.43 %	1.72 %	0.83 %	0.25 %
0 °C	First-Order RC ECM	17.69 %	65.63 %	29.07 %	17.64 %	13.62 %
	Hybrid model	9.14 %	12.99 %	21.17 %	12.31 %	5.08 %
−10 °C	First-Order RC ECM	33.96 %	49.90 %	49.55 %	18.55 %	35.45 %
	Hybrid model	4.33 %	0.58 %	22.27 %	15.32 %	20.63 %

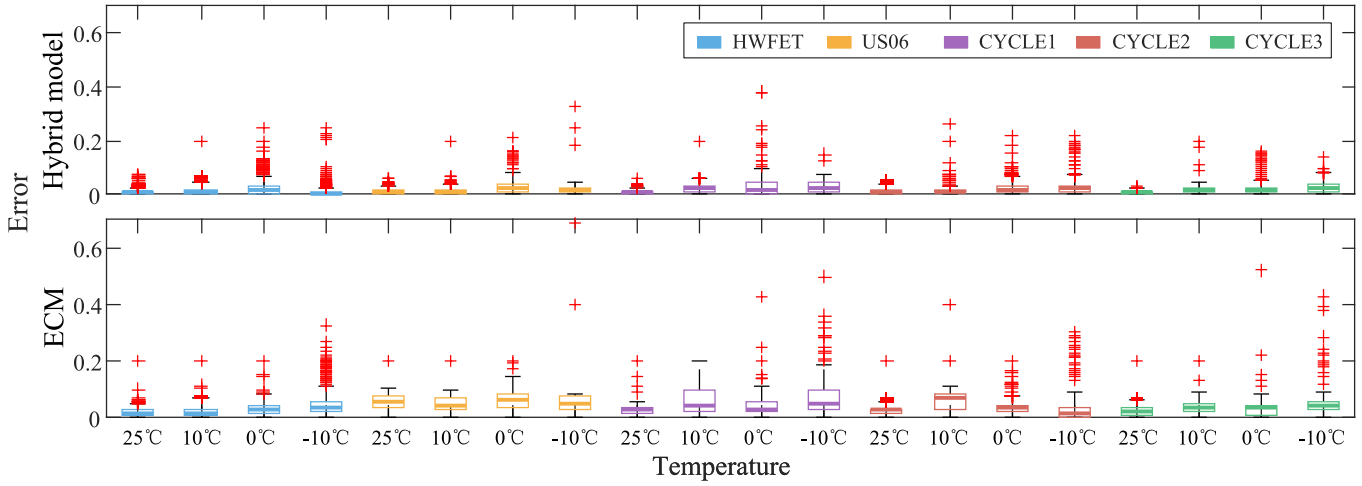

Fig. 12. Boxplot analysis of SOC estimation error distributions between Hybrid model and First-Order RC ECM.

provided by [35]. This dataset includes a commercial LFP ($LiFePO_4$) cell with an 18,650 form factor, charged at 0.5C and discharged at 1C at 25 °C. It contains data from 3,544 charge–discharge cycles. Details of the battery is shown in Table 8.

The SOH of a battery is defined as the ratio of the maximum discharge capacity during the current cycle to the rated capacity

Table 5
RMSE and MAPE comparison of SOC estimation results.

Temp	Comparison models	Operating condition				
		HWFET	US06	CYCLE1	CYCLE2	CYCLE3
25 °C	ECM	RMSE: 0.0227 MAPE: 6.41 %	RMSE: 0.0638 MAPE:16.56 %	RMSE: 0.0302 MAPE: 7.00 %	RMSE: 0.0324 MAPE: 8.04 %	RMSE: 0.0311 MAPE: 5.69 %
	Hybrid model	RMSE: 0.0186 MAPE: 3.86 %	RMSE: 0.0157 MAPE: 3.34 %	RMSE: 0.0113 MAPE: 3.39 %	RMSE: 0.0185 MAPE: 4.01 %	RMSE: 0.0120 MAPE: 2.84 %
	Improvement (RMSE)	18.06 %	75.39 %	62.58 %	42.90 %	61.41 %
10 °C	ECM	RMSE: 0.0276 MAPE: 6.69 %	RMSE: 0.0542 MAPE: 11.70 %	RMSE: 0.0703 MAPE: 15.68 %	RMSE: 0.0679 MAPE: 13.46 %	RMSE: 0.0392 MAPE: 7.26 %
	Hybrid model	RMSE: 0.0202 MAPE: 3.59 %	RMSE: 0.0193 MAPE: 3.21 %	RMSE: 0.0245 MAPE: 3.96 %	RMSE: 0.0176 MAPE: 2.63 %	RMSE: 0.0228 MAPE: 3.58 %
	Improvement (RMSE)	26.81 %	64.39 %	65.15 %	74.08 %	41.84 %
0 °C	ECM	RMSE: 0.0379 MAPE: 7.63 %	RMSE: 0.0590 MAPE: 14.53 %	RMSE: 0.0479 MAPE: 7.60 %	RMSE: 0.0421 MAPE: 6.29 %	RMSE: 0.0426 MAPE: 4.70 %
	Hybrid model	RMSE: 0.0262 MAPE: 3.80 %	RMSE: 0.0363 MAPE: 3.85 %	RMSE: 0.0328 MAPE: 3.47 %	RMSE: 0.0290 MAPE: 3.73 %	RMSE: 0.0307 MAPE: 2.83 %
	Improvement (RMSE)	30.87 %	38.47 %	31.52 %	31.12 %	27.93 %
−10 °C	ECM	RMSE: 0.0653 MAPE: 7.62 %	RMSE: 0.0663 MAPE: 9.56 %	RMSE: 0.0743 MAPE: 11.89 %	RMSE: 0.0456 MAPE: 4.49 %	RMSE: 0.0542 MAPE: 7.63 %
	Hybrid model	RMSE: 0.0259 MAPE: 2.63 %	RMSE: 0.0318 MAPE: 3.93 %	RMSE: 0.0375 MAPE: 3.83 %	RMSE: 0.0384 MAPE: 3.73 %	RMSE: 0.0370 MAPE: 3.90 %
	Improvement (RMSE)	60.34 %	52.04 %	49.53 %	15.79 %	31.73 %

Table 6
Time for offline training and online SOC estimation.

Condition	Offline training time (s)		Online SOC estimation time (s)	
	Hybrid model	First-Order RC ECM	Hybrid model	First-Order RC ECM
HWFET	450.088	1.804	2.243	2.349
US06	263.940	1.560	1.325	1.167
CYCLE1	572.833	2.061	2.864	2.773
CYCLE2	550.947	1.983	2.759	2.865
CYCLE3	594.364	2.267	2.904	2.844

Table 7A
Modeling accuracy (terminal voltage RMSE) of the hybrid model on CYCLE2 and CYCLE3.

	25 °C	10 °C	0 °C	−10 °C
CYCLE2	0.0947	0.0748	0.0483	0.0932
CYCLE3	0.0752	0.0641	0.0477	0.1022

$$SOH = \frac{C_{current}}{C_{rated}} \times 100\% \tag{25}$$

where $C_{current}$ is the maximum discharge capacity during the current cycle, C_{rated} is the rated capacity of the battery.

Discharge data from multiple charge–discharge cycles were selected at approximately 500-cycle intervals to validate the model's accuracy across different stages of cycle aging. Similar to Section 4.1, the RMSE is used to evaluate the modeling accuracy of the terminal voltage by comparing the model's predictions to the true values. For the accuracy of the SOC estimation, both RMSE and MAPE are employed to compare the model's estimates to the true SOC values. Table 9 compares the modeling accuracy and SOC estimation results between the hybrid model and First-Order RC ECM at different stages of cycle aging.

Fig. 14 shows the RMSE improvement of the hybrid model compared to First-Order RC ECM in modeling accuracy and SOC estimation.

The results support these observations:

The battery parameters change dynamically with cycle aging. When in the 85 %–90 % SOH range, the modeling accuracy of the First-Order RC ECM decreases significantly, leading to reduced accuracy in SOC estimation. The introduction of FreTS modules effectively mitigates this issue. In the 85 %–95 % SOH range, the average modeling accuracy is characterized by a RMSE of 0.0239, representing a 21.98 % improvement. The average SOC estimation accuracy is further improved, with RMSE values of 0.0060 for SOH in the 90 %–95 % range and 0.0122 for SOH in the 85 %–90 % range, representing a 62.27 % average improvement.

Table 7B
SOC estimation performance of the hybrid model on CYCLE2 and CYCLE3.

	25 °C	10 °C	0 °C	−10 °C
CYCLE2	RMSE: 0.0127 MAPE: 3.98 %	RMSE: 0.0212 MAPE: 3.66 %	RMSE: 0.0228 MAPE: 2.51 %	RMSE: 0.0305 MAPE: 4.74 %
CYCLE3	RMSE: 0.0164 MAPE: 3.04 %	RMSE: 0.0237 MAPE: 3.81 %	RMSE: 0.0263 MAPE: 4.21 %	RMSE: 0.0248 MAPE: 3.53 %

Table 8
LFP ($LiFePO_4$) cell information.

Parameter	Value
Nominal Capacity (Ah)	1.1
Nominal Voltage (V)	3.3
Voltage Range (V)	2 to 3.6
Max Discharge Current (A)	30

5. Conclusions

In this paper, a hybrid model is proposed for lithium-ion batteries to enhance the state estimation accuracy under complex operating conditions. Three FreTS modules are embedded into the classical First-Order RC ECM, serving as "virtual electronic components" to increase the nonlinear-fitting ability and adaptability. To train the embedded FreTS modules, an iterative training process is designed to convert the indirect training problem into a typical regression problem. Particularly, the battery state space equation is merged into the MSE loss to formulate a physics-informed loss function that enables the FreTS modules training. Simulations are conducted based on two real-world battery datasets. The first dataset contains 20 scenarios (under 5 different operating conditions at 4 different ambient temperatures), the second dataset contains the discharge data of the battery at 85 %–95 % SOH. The results under different temperatures and complex operating conditions show that the proposed method improves RMSE by 6 %–40 % in modeling accuracy and 18 %–75 % in SOC estimation compared to the First-Order RC ECM. Under various aging cycles, the method achieves a 22 % RMSE improvement in modeling accuracy and a 62 % improvement in SOC estimation. Due to the lightweight nature of FreTS modules, the hybrid model exhibits an average offline training time of 486 s and online SOC estimation time of 2.419 s under various operating conditions, which is considered sufficient enough to be implemented in real-world scenarios.

Future work may focus on trying to establish hybrid model based on

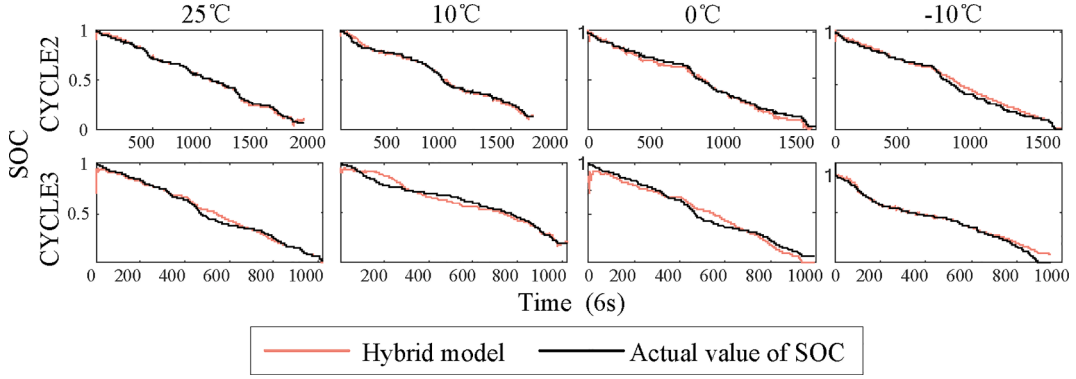

Fig. 13. Cross-cycle SOC estimation under different temperatures.

Table 9
RMSE and MAPE comparison between hybrid model and First-Order RC ECM.

Cycle			2	503	1010	1516	2024	2533	3035	3542
SOH			94.00	92.55	91.55	90.36	89.27	88.09	87.00	85.81
Modeling accuracy	ECM (RMSE)		0.0277	0.0331	0.0251	0.0239	0.0239	0.0389	0.0359	0.0364
	Hybrid model (RMSE)		0.0248	0.0257	0.0239	0.0223	0.0225	0.0255	0.0241	0.0222
SOC estimation	ECM	RMSE	0.0133	0.0106	0.0249	0.0227	0.0151	0.0343	0.0393	0.0399
		MAPE	2.93 %	2.18 %	5.14 %	4.52 %	2.64 %	6.04 %	7.75 %	7.95 %
	Hybrid model	RMSE	0.0099	0.0023	0.0049	0.0068	0.0105	0.0117	0.0145	0.0120
		MAPE	2.15 %	0.36 %	0.82 %	1.24 %	2.04 %	1.89 %	2.75 %	1.92 %

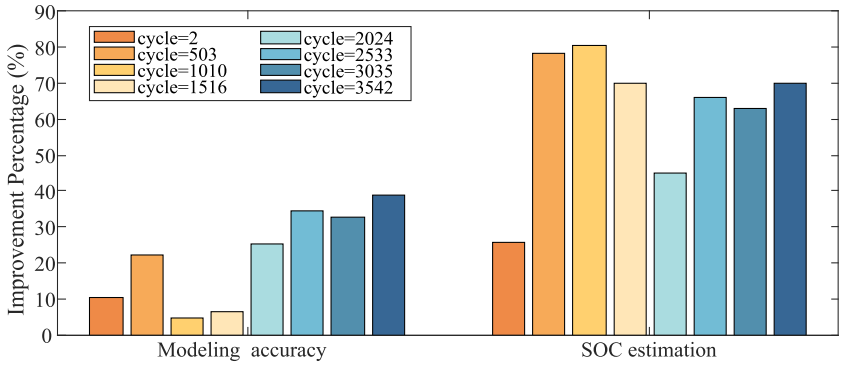

Fig. 14. The improvement of hybrid model in modeling accuracy and SOC estimation compared with First-Order RC ECM.

higher-order ECMs to improve the overall performance.

CRediT authorship contribution statement

Zelin Guo: Writing – original draft, Visualization, Validation, Software, Methodology, Investigation, Formal analysis. **Yiyan Li:** Writing – review & editing, Supervision, Project administration, Funding acquisition, Conceptualization. **Zhenghao Zhou:** Software, Investigation. **Chen Zhang:** Supervision, Methodology. **Zheng Yan:** Methodology, Formal analysis. **Mo-Yuen Chow:** Methodology, Conceptualization.

Declaration of competing interest

The authors declare that they have no known competing financial interests or personal relationships that could have appeared to influence the work reported in this paper.

Acknowledgment

This work was supported by National Natural Science Foundation of China under Grant 52307121.

Data availability

Data will be made available on request.

References

[1] Taheri AH, Ardehali MM. Optimal design and management of renewable energy system for charging infrastructure of hydrogen fuel cell and battery electric vehicles. Energ Conver Manage 2025;326:119415. https://doi.org/10.1016/j.enconman.2024.119415.
[2] Qays MO, Buswig Y, Hossain ML, Abu-Siada A. Recent progress and future trends on the state of charge estimation methods to improve battery-storage efficiency: a review. CSEE J Power Energy Syst 2022;8(1):105–14. https://doi.org/10.17775/CSEEJPES.2019.03060.
[3] Nejad S, Gladwin DT, Stone DA. A systematic review of lumped-parameter equivalent circuit models for real-time estimation of lithium-ion battery states. J Power Sources 2016;316:183–96. https://doi.org/10.1016/j.jpowsour.2016.03.042.
[4] How DNT, Hannan MA, Hossain Lipu MS, Ker PJ. State of charge estimation for lithium-ion batteries using model-based and data-driven methods: a review. IEEE Access 2019;7:136116–36. https://doi.org/10.1109/ACCESS.2019.2942213.
[5] Mama M, Solai E, Capurso T, Danlos A, Khelladi S. Comprehensive review of multi-scale lithium-ion batteries modeling: from electro-chemical dynamics up to heat transfer in battery thermal management system. Energ Conver Manage 2025;325:119223. https://doi.org/10.1016/j.enconman.2024.119223.
[6] Liaw BY, Nagasubramanian G, Jungst RG, Doughty DH. Modeling of lithium ion cells—a simple equivalent-circuit model approach. Solid State Ion 2004;175:835–9. https://doi.org/10.1016/j.ssi.2004.09.049.
[7] Dubarry M, Liaw BY. Development of a universal modeling tool for rechargeable lithium batteries. J Power Sources 2007;174:856–60. https://doi.org/10.1016/j.jpowsour.2007.06.157.
[8] Freeborn TJ, Maundy B, Elwakil AS. Fractional-order models of supercapacitors, batteries and fuel cells: a survey. Mater Renew Sustain Energy 2015;4. https://doi.org/10.1007/s40243-015-0052-y.
[9] Obeid H, Petrone R, Chaoui H, Gualous H. Higher order sliding-mode observers for state-of-charge and state-of-health estimation of lithium-ion batteries. IEEE Trans Veh Technol 2023;72(4):4482–92. https://doi.org/10.1109/TVT.2022.3226686.
[10] Zhang W, Wang L, Wang L, Liao C, Zhang Y. Joint state-of-charge and state-of-available-power estimation based on the online parameter identification of lithium-ion battery model. IEEE Trans Ind Electron 2022;69(4):3677–88. https://doi.org/10.1109/TIE.2021.3073359.
[11] Yun J, Choi Y, Lee J, Choi S, Shin C. State-of-charge estimation method for lithium-ion batteries using extended Kalman filter with adaptive battery parameters. IEEE Access 2023;11:90901–15. https://doi.org/10.1109/ACCESS.2023.3305950.
[12] Shen P, Ouyang M, Lu L, Li J, Feng X. The co-estimation of state of charge, state of health, and state of function for lithium-ion batteries in electric vehicles. IEEE Trans Veh Technol 2018;67(1):92–103. https://doi.org/10.1109/TVT.2017.2751613.
[13] Liu S, Dong X, Zhang Y. A new state of charge estimation method for lithium-ion battery based on the fractional order model. IEEE Access 2019;7:122949–54. https://doi.org/10.1109/ACCESS.2019.2932142.
[14] Hu X, Yuan H, Zou C, Li Z, Zhang L. Co-estimation of state of charge and state of health for lithium-ion batteries based on fractional-order calculus. IEEE Trans Veh Technol 2018;67(11):10319–29. https://doi.org/10.1109/TVT.2018.2865664.
[15] Yang D, Wang Y, Pan R, Chen R, Chen Z. State-of-health estimation for the lithium-ion battery based on support vector regression. Appl Energy 2018;227:273–83. https://doi.org/10.1016/j.apenergy.2017.08.096.
[16] Chemali E, Kollmeyer PJ, Preindl M, Emadi A. State-of-charge estimation of Li-ion batteries using deep neural networks: a machine learning approach. J Power Sources 2018;400:242–55. https://doi.org/10.1016/j.jpowsour.2018.06.104.
[17] Zhang L, Zheng M, Du D, Li Y, Fei M, Guo Y, Li K, Na J. State-of-charge estimation of lithium-ion battery pack based on improved RBF neural networks. Complex 2020;2020. https://doi.org/10.1155/2020/8840240.
[18] Chaoui H, Ibe-Ekeocha CC. State of charge and state of health estimation for lithium batteries using recurrent neural networks. IEEE Trans Veh Technol 2017;66(10):8773–83. https://doi.org/10.1109/TVT.2017.2715333.

[19] Yang F, Song X, Xu F, Tsui K-L. State-of-charge estimation of lithium-ion batteries via long short-term memory network. IEEE Access 2019;7:53792–9. https://doi.org/10.1109/ACCESS.2019.2912803.
[20] Aihua T, Huang Y, Liu S, Yu Q, Shen W, Xiong R. A novel lithium-ion battery state of charge estimation method based on the fusion of neural network and equivalent circuit models. Appl Energy 2023;348:121578. https://doi.org/10.1016/j.apenergy.2023.121578.
[21] Kuzhiyil JA, Damoulas T, Widanage WD. Neural equivalent circuit models: Universal differential equations for battery modelling. Appl Energy 2024;371:123692. https://doi.org/10.1016/j.apenergy.2023.123692.
[22] Luzi M, Mascioli FMF, Paschero M, Rizzi A. A white-box equivalent neural network circuit model for SoC estimation of electrochemical cells. IEEE Trans Neural Networks Learn Syst 2019;31(2):371–82. https://doi.org/10.1109/TNNLS.2019.2901439.
[23] Brucker J, Gasper R, Bessler WG. A grey-box model with neural ordinary differential equations for the slow voltage dynamics of lithium-ion batteries: application to single-cell experiments. J Power Sources 2024;614:234918. https://doi.org/10.1016/j.jpowsour.2023.234918.
[24] Ma M, Hu J, Xiao R. Energy management strategy with model prediction for fuel cell hybrid trucks considering vehicle mass and road slope. Energ Conver Manage 2025;333:119791. https://doi.org/10.1016/j.enconman.2025.119791.
[25] Yi K, Zhang Q, Fan W, Wang S, Wang P, He H, et al. Frequency-domain MLPs are more effective learners in time series forecasting. Adv Neural Inf Proces Syst 2023;36:76656–79.
[26] Yun B, Dong W, Wang D. Online internal resistance measurement application in lithium ion battery capacity and state of charge estimation. Energies 2018;11. https://doi.org/10.3390/en11051073.
[27] Mohamed A, Ehrensberger M, Scheuer R, Endisch C, Lewerenz M. Long-Term Self-Discharge Measurements and Modelling for Various Cell Types and Cell Potentials. Energies 2023;16. https://doi.org/10.3390/en16093889.
[28] Cui Z, Hu W, Zhang G, Zhang Z, Chen Z. An extended Kalman filter based SOC estimation method for Li-ion battery. Energy Rep 2022;8:81–7. https://doi.org/10.1016/j.egyr.2022.02.116.
[29] Adedeji BP, Kabir G. A feedforward deep neural network for predicting the state-of-charge of lithium-ion battery in electric vehicles. Decis Anal J 2023;8. https://doi.org/10.1016/j.dajour.2023.100255.
[30] Phillip K. Panasonic 18650PF Li-ion battery data. Mendeley Data 2018;V1. https://doi.org/10.17632/wykht8y7tg.1.
[31] U.S. Environmental Protection Agency. Highway fuel economy test (HWFET). EPA; 1978.
[32] U.S. Environmental Protection Agency. U.S. 06 driving cycle (US06). EPA; 2005.
[33] U.S. Environmental Protection Agency. Urban Dynamometer Driving Schedule (UDDS) test procedure. EPA; 1978.
[34] U.S. Environmental Protection Agency. Los Angeles 92 driving cycle (LA92). EPA; 1992.
[35] Preger Y, Barkholtz HM, Fresquez A, Campbell DL, Juba BW, Romàn-Kustas J, et al. Degradation of commercial lithium-ion cells as a function of chemistry and cycling conditions. J Electrochem Soc 2020;167(12):120532. https://doi.org/10.1149/1945-7111/abae37.